

This paper is published as : El Jisr, H., Elkady, A., Lignos, D.G. (2019). “Composite steel beam database for seismic design and performance assessment of composite-steel moment-resisting frame systems, Bulletin of Earthquake Engineerin, Vol. 17(6), pp. 3015-3039, doi: 10.1007/s10518-019-00564-w.

Composite steel beam database for seismic design and performance assessment of composite-steel moment-resisting frame systems

Hammad El Jisr · Ahmed Elkady · Dimitrios G. Lignos

Abstract This paper discusses the development of a publicly available database of composite steel beam-to-column connections under cyclic loading. The database is utilized to develop recommendations for the seismic design and nonlinear performance assessment of steel and composite-steel moment-resisting frames (MRFs). In particular, the sagging/hogging plastic flexural resistance as well as the effective slab width are assessed through a comparison of the European, US and Japanese design provisions. The database is also used to quantify the plastic rotation capacity of composite steel beams under sagging/hogging bending. It is found that the Eurocode 8-Part 3 provisions overestimate the plastic rotation capacities of composite beams by 50% regardless of their web slenderness ratio. Empirical relationships are developed to predict the plastic rotation capacity of composite steel beams as a function of their geometric and material properties. These relationships can facilitate the seismic performance assessment of new and existing steel and composite-steel MRFs through nonlinear static analysis. The collected data underscores that the beam-to-column web panel zone in composite steel beam-to-column connections experience higher shear demands than their non-composite counterparts. A relative panel zone-to-beam resistance ratio is proposed that allows for controlled panel zone inelastic deformation of up to 10 times the panel zone’s shear yield distortion angle. Notably, when this criterion was imposed, there was no fracture in all the examined beam-to-column connections.

Keywords Composite steel beam database · seismic performance assessment · composite floors · Plastic rotation capacity · Panel zone shear resistance

H. El Jisr . A. Elkady . D. G. Lignos (✉)

School of Architecture Civil and Environmental Engineering, École Polytechnique Fédérale de Lausanne, Lausanne, Switzerland

e-mail: dimitrios.lignos@epfl.ch

tel: +41 21 69 32427

1. Introduction

Modern seismic design provisions adopt capacity design principles that allow for controlled inelastic deformations within a lateral-load resisting system (Fardis 2018). In the case of steel and composite-steel moment-resisting frame (MRF) systems, steel beams act as the primary structural fuse to dissipate the seismic energy. Prior studies (Lignos et al. 2013; Elkady and Lignos 2014, 2015) suggest that the amplified flexural resistance of composite steel beams could shift the plastic hinge formation to the MRF columns despite the fact that a strong-column/weak-beam (SCWB) criterion was imposed. Subassembly tests on deep beams (depth, $h = 913$ mm) with partial composite action (Uang et al. 2000; Jones et al. 2002), showed that their sagging flexural resistance (i.e. slab in compression) amplified by about 10% to 20% relative to the bare beam plastic bending resistance. Similarly, beams with a depth of 753 mm tested by Civjan et al. (2001) developed a sagging flexural resistance amplification of 10% to 30%. Elkady and Lignos (2014) assessed the hysteretic behavior of composite steel beams with reduced beam section (RBS) with depths varying between 533 mm and 911 mm. These sizes are typically used in perimeter steel MRFs in North America. They found that the composite slab amplifies the sagging flexural resistance, on average, by 35%. In Japan and Europe, the use of space steel MRFs is promoted. This typically leads to the selection of shallow beams ($h = 300$ to 500 mm) even in tall buildings (Nakashima et al. 2000; Mele 2002). The amplification of the sagging flexural resistance in such beams is even more pronounced. In particular, Nakashima et al. (2007) showed that the composite action amplifies the sagging flexural resistance of 400 mm deep beams by up to 50%. This agrees with prior experimental studies (Bursi and Gramola 2000; Bursi et al. 2009).

The potential deficiencies associated with disregarding the composite action in seismic design can be alleviated by (a) totally disconnecting the slab from the column face (Tremblay et al. 1997); (b) by employing a larger SCWB ratio (Elkady and Lignos 2014); or (c) by explicitly considering the expected composite beam flexural resistance in the SCWB check. The European (CEN 2004a), American (AISC 2016a) and Japanese (AIJ 2010a) seismic design provisions compute the flexural resistance of composite steel beams differently. The main two reasons are the variations in the assumed effective width of the slab and the shear strength of the studs. The sensitivity of the flexural resistance of composite steel beams to the above assumptions has not been consistently quantified through direct comparisons with available experimental data.

Nonlinear modeling recommendations (e.g. ASCE/SEI 41-17 and Eurocode 8-Part 3) for the seismic assessment of new and existing structures (ASCE 2017; CEN 2005a) compute a beam's elastic flexural stiffness and plastic rotation capacity by ignoring the composite action. Nam and Kasai (2012) analyzed data from full-scale shake table experiments (Suita et al. 2008; Lignos et al. 2013) and showed that the presence of the slab may increase the beam stiffness by two to three times. Similarly, system-level tests (Nakashima et al. 2007) indicated that the composite steel beam stiffness was twice as high compared to that of a non-composite beam. Prior subassembly tests (Engelhardt et al. 2000; Roeder 2000; Zhang et al. 2004) suggest that, depending on the slab arrangement and the associated degree of composite action, the plastic rotation capacity of a composite steel beam under sagging bending could be up to 80% larger than that of a non-composite beam. In a more recent study, Elkady and Lignos (2014) assessed the plastic rotation capacity of composite deep beams with RBS. These experience an 80% and 35% increase in the pre- and post-capping plastic rotations, respectively, compared to non-composite steel beams (capping refers here to the onset of local and/or member geometrical instabilities). However, the above data-set did not cover shallow beams commonly seen in the European and Japanese design practice. This is particularly important for seismic performance assessment methodologies consistent with Eurocode 8-Part 3 (CEN 2005a).

A side issue related to the composite action effects is the increase in the shear demand on the beam-to-column web panel zone (Leon et al. 1998; Elkady and Lignos 2014). This could augment the panel zone inelastic deformations. It is desirable to allow for controlled panel zone inelastic deformation (Krawinkler 1978; Shin and Engelhardt 2013). While moderate levels of inelastic deformation are usually permitted within the various seismic design provisions in Europe, North America and Asia, there is no consensus on what an acceptable panel zone inelastic deformation range should be.

This paper presents the development of a comprehensive experimental database for composite steel beams that addresses all the aforementioned issues. The database is used to assess several parameters that influence the cyclic behavior of composite steel beams in fully restrained beam-to-column connections. These parameters include (i) the flexural resistance, (ii) the effective stiffness, and (iii) the pre- and post-capping plastic rotation capacities. The gathered experimental data is also used to assess the shear resistance of the beam-to-column web panel in composite beam-to-column connections. Three design provisions are considered including the European [Eurocode 3, 4 and 8 (CEN 2004a, b; 2005a, b, c)]; the US (ANSI/AISC 360-16 (AISC 2016b) and ANSI/AISC 341-16 (AISC 2016a)]; and the Japanese (AIJ 2010a, b) provisions. The paper proposes a set of seismic design recommendations for composite-steel MRFs that can be adopted in future design

This paper is published as : El Jisr, H., Elkady, A., Lignos, D.G. (2019). “Composite steel beam database for seismic design and performance assessment of composite-steel moment-resisting frame systems, Bulletin of Earthquake Engineering, Vol. 17(6), pp. 3015-3039, doi: 10.1007/s10518-019-00564-w.

provisions. Finally, nonlinear modeling recommendations are also proposed for estimating the flexural resistance, stiffness and plastic rotation capacity of composite steel beams. These recommendations can facilitate the seismic performance assessment of existing steel frame buildings as well as prospective designs.

2. Description of the Assembled Composite Steel Beam Database

The assembled composite steel beam database comprises 24 experimental programs, which are summarized in Table 1. A total of 97 composite steel beams are gathered including 87 from subassembly tests and 10 from system-level experiments. The beam depths, h , range from 300 to 912 mm; shear span-to-depth ratios, L_o/h (L_o is the distance from the column face to the inflection point) range from 3.4 to 11.6; and web slenderness ratios, c/t_w , range from 36.1 to 53.8. Both partially- and fully-composite steel beam data were gathered. The main beam-to-column connections include:

- Bolted extended end-plate connections (BEEP) (see Fig. 1a)
- Welded unreinforced flange welded web connections (WUF-W) (see Fig. 1b)
- Reduced beam section connections (RBS) (see Fig. 1c)
- Through diaphragm connections (TD) (see Fig. 1d)
- Retrofitted connections (bottom flange RBS, top and/or bottom welded or bolted haunches, bottom flange horizontal stiffeners, bottom flange cover plate)
- Reinforced concrete column with steel beams (RCS) and concrete filled steel tube (CFT) steel beam-to-column connections

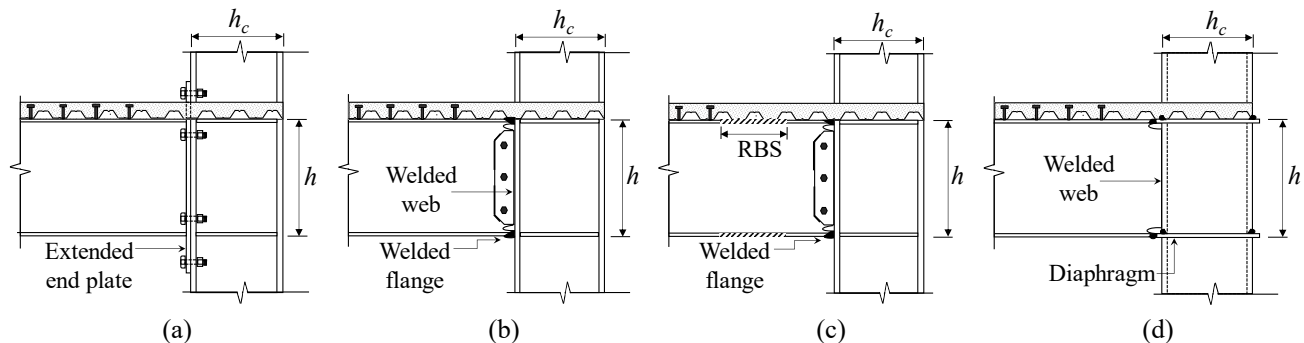
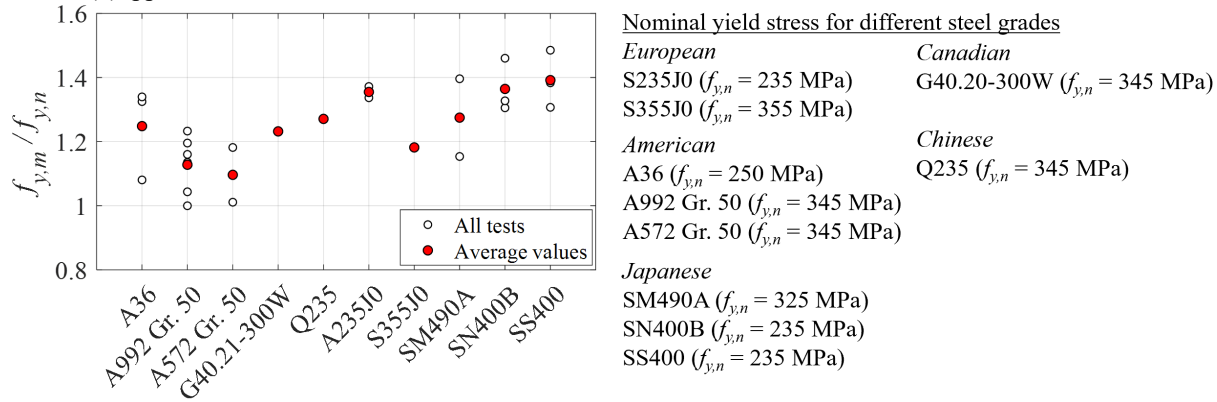


Fig. 1. Typical fully restrained beam-to-column connection types included in the composite steel beam database: (a) BEEP; (b) WUF-W; (c) RBS; (d) TD connection

The collected steel beams are made of 10 steel material types. The measured-to-nominal yield stress ratio ($f_{y,m} / f_{y,n}$) for each steel type is plotted in Fig. 2, which summarizes the nominal yield stress values. This ratio varies from an average minimum of 1.1 for US A572 Gr.50 steel to an average maximum of 1.4 for Japanese SS400 steel. The values are consistent with the material overstrength values reported in ANSI/AISC 341-16 (AISC 2016a) for US steel grades, the OPUS¹ program (Braconi et al. 2013) for European steel grades, and in Fujisawa et al. (2013) for Japanese steel grades. The measured 28-day concrete compressive strength of the concrete slabs varies between 15 to 40 MPa. In summary, the composite steel beam database is publicly available online at <http://resslabtools.epfl.ch/steel>.

¹ Optimizing the seismic performance of steel and steel-concrete structures by standardizing material quality control



133 **Fig. 2.** Ratio of measured-to-nominal yield stress of the various steel types in the assembled database
 134 **Table 1.** Summary of the composite steel beam testing programs in the assembled database

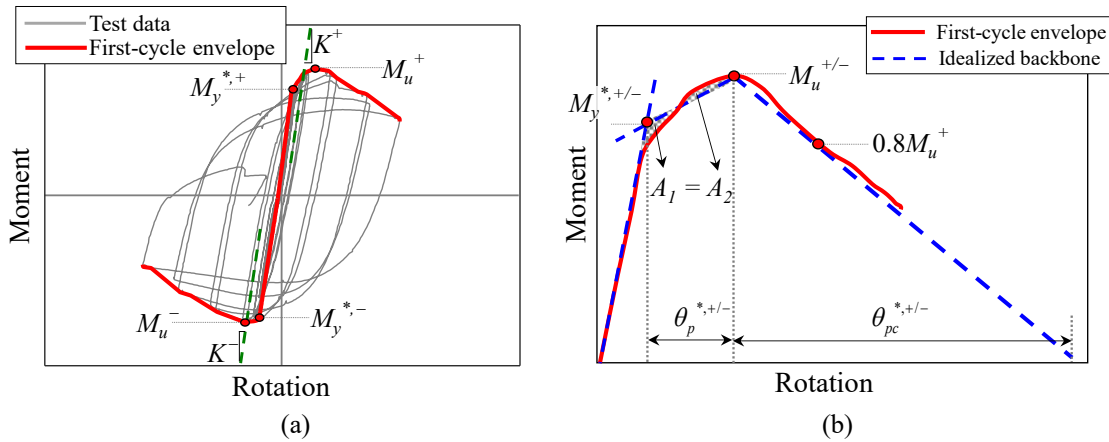
Reference	Connection Type	h [mm]	Floor Slab*	Steel Grade	$\frac{L_o}{h}$	$\frac{c}{t_w}$
Zhang et al. (2004)	RBS	760/911	NWC -	A572/A992 Gr. 50	4.4/5.5	51.9/47.6
Chen and Chao (2001)	RBS	600	NWC -	A36	4.4	44.2
Civjan et al. (2001)	Retrofit	755	LWC - \perp	A36	4.6	51.5
Leon et al. (1998)	WUF-W	683	NWC -	A36	4.9	48.6
Engelhardt et al. (2000)	RBS	911	NWC -	A572 Gr. 50	3.9	51.9
Tremblay et al. (1997)	RBS	535	NWC - \perp	G40.21-300W	6.8	45.7
Ricles et al. (2002)	WUF-W	911	NWC -	A572 Gr. 50	4.7	51.9
Cheng et al. (2007)	CFT	450	NWC -	not reported	6.3	44.0
Cheng and Chen (2005)	RCS	596	NWC -	not reported	4.5	53.8
Uang et al. (2000)	Retrofit	911	LWC - \perp	A36	3.4	51.9
Kim et al. (2004)	TD	612	NWC - SS	SM490	5.4	41.5
Yamada et al. (2009)	TD	400	NWC -	SN400B	5.9	43.5
Nakashima et al. (2005)	TD	400	NWC -	A572 Gr. 50	7.1	38.0
Nakashima et al. (2007)	TD	400	NWC -	SN400B	5.8	38.0
Cordova & Deierlein (2005)	RCS	600	NWC - NR	A572 Gr. 50	5.3	47.8
Bursi et al. (2009)	RCS	400	NWC -	S355	5.9	38.5
Kishiki et al. (2010)	TD	300	NWC - SS, , \perp	SM490A/SN400B	5.4	39.4
Sumner & Murray (2002)	BEEP	600	NWC -	A572 Gr. 50	5.2	50.6
Bursi et al. (2009)	WUF-W	330	NWC -	S235	11.6	36.1
Kim and Lee (2017)	Retrofit	500	NWC - \perp	SS400	7.6	44.2
Lee et al. (2016)	WUF-W/RBS	350	NWC - \perp	SS400	6.0	51.3
Lu et al. (2017)	RBS	350	NWC - SS	Q235	4.3	43.1
Asada et al. (2015)	TD	400	NWC - \perp	SS400	10.6	43.5
Del Carpio et al. (2014)	RBS	350	NWC -	A572 Gr. 50	6.0	48.1

*NWC: Normal-weight concrete
 LWC: Light-weight concrete
 SS: Solid slab with no steel deck

||: Deck with ribs parallel to the beam
 \perp : Deck with ribs perpendicular to the beam

3. Deduced Performance Parameters of Composite Steel Beams under Cyclic Loading

138 A number of performance parameters are deduced from manually digitized and processed moment-rotation relations of
 139 the collected data-set. An example is illustrated in Fig. 3. In this figure, the *moment* corresponds to that at the idealized
 140 center of the beam’s plastic hinge region. The *rotation* represents the beam’s rotation over its length (chord rotation). These
 141 definitions are consistent with those found in ASCE/SEI 41-17 (ASCE 2017). Referring to Fig. 3a, a first-cycle envelope
 142 curve is first fitted to the moment-rotation relation data in both the positive (i.e., sagging bending) and negative (i.e., hogging
 143 bending) loading directions. These curves are then used to deduce a number of parameters that characterize the stiffness,
 144 flexural strength and plastic deformation capacity of a composite beam. The deduced parameters include the effective
 145 stiffness ($K^{+/-}$), the effective plastic flexural resistance ($M_y^{*,+/-}$), the ultimate flexural resistance ($M_u^{+/-}$), and the pre- and
 146 post-capping plastic rotation capacities ($\theta_p^{*,+/-}$ and $\theta_{pc}^{*,+/-}$, respectively). The star (*) superscript denotes that these
 147 parameters are based on the first-cycle envelope curve. Therefore, they are distinguished from those that define a monotonic
 148 backbone of a steel beam. The effective stiffness is systematically derived from the unloading stiffness of the first inelastic
 149 cycle excursion, which by definition includes both flexural and shear deformations; thus, the term “effective” is adopted.
 150 The flexural resistance and rotation parameters are deduced from a tri-linear idealized curve (see dashed lines in Fig. 3b)
 151 fitted to the first-cycle envelope. The idealized curve is fitted such that the total energy dissipated up to the peak response
 152 ($M_u^{+/-}$) is the same as that in the tri-linear approximation. Albeit the extracted plastic rotation values are loading-history
 153 dependent (Krawinkler 2009), they are consistent with prior related studies (Panagiotakos and Fardis 2001) that are already
 154 adopted in Eurocode 8-Part 3 (CEN 2005a) and ASCE (2017). The subsequent sections provide a comprehensive assessment
 155 of the deduced performance parameters in comparison with relevant seismic code design provisions and performance
 156 assessment guidelines for nonlinear static analysis procedures.
 157



158 **Fig. 3.** Definition of performance parameters for composite steel beams under cyclic loading

159
 160 **3.1. Sagging Resistance**
 161

162 The deduced effective plastic flexural resistance of composite steel beams under sagging bending (simply noted as
 163 sagging resistance hereafter) is assessed based on 46 data points. These represent beams that reached their ultimate flexural
 164 resistance. Beams that experienced premature fracture were excluded from the data-set. The test data suggests that the
 165 sagging resistance amplification due to the composite action is mainly dependent on the beam depth, the shear span-to-
 166 depth ratio and the degree of composite action, η , which is defined in Eq. (1). In particular, η is the ratio of the actual
 167 number of used shear studs to that required ones to achieve full composite action.
 168

169
$$\eta = \frac{\sum F_v}{\min\{F_c, N_{pl}\}} \leq 1 \quad (1)$$

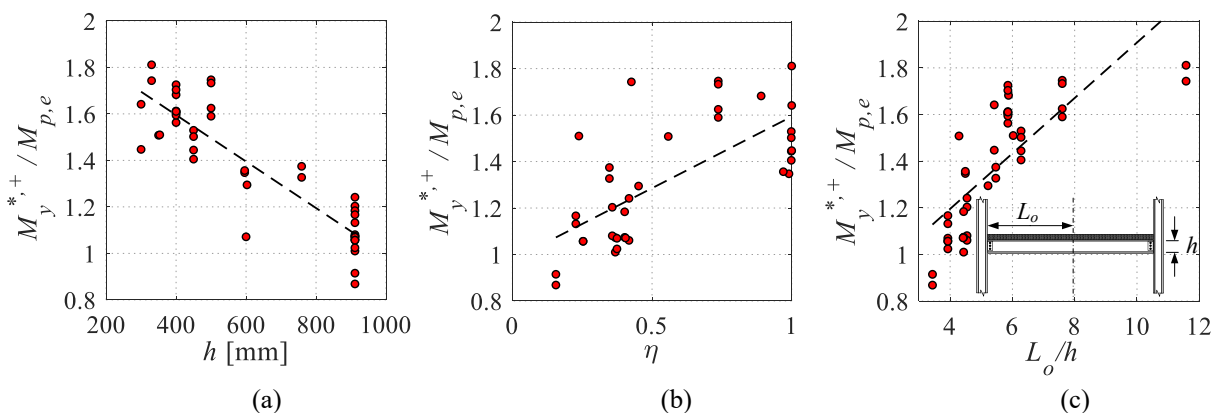
170 in which $\sum F_v$ is the shear strength of the headed shear studs between the point of maximum positive moment and the point
 171 of zero moment based on the respective code, F_c is the compressive strength of the slab at the crushing limit state, and N_{pl}
 172 is the tensile plastic resistance of the steel section based on measured material properties.
 173

This paper is published as : El Jisr, H., Elkady, A., Lignos, D.G. (2019). “Composite steel beam database for seismic design and performance assessment of composite-steel moment-resisting frame systems, Bulletin of Earthquake Engineering, Vol. 17(6), pp. 3015-3039, doi: 10.1007/s10518-019-00564-w.

174 The aforementioned dependencies are assessed by plotting the sagging resistance with respect to the aforementioned
 175 parameters. The sagging resistance is normalized with respect to the bare steel beam’s expected plastic flexural resistance,
 176 $M_{p,e}$ ($M_{p,e}$ is the product of the plastic section modulus of the respective beam about the strong axis and the expected yield
 177 stress of the beam steel material, $f_{y,e}$). the $f_{y,e}$ is deduced based on the material’s expected-to-nominal yield stress ratio, R_y ,
 178 which is obtained from ANSI/AISC 341-16 (AISC 2016a) for North American steel grades and from available literature
 179 (Hirofumi and Masayuki 1985; Braconi et al. 2013; Fujisawa et al. 2013) for the rest of the steel grades.

180 Figure 4a shows that the sagging resistance is amplified by 13%, on average, for deep beams ($h > 500$ mm). On the other
 181 hand, the sagging resistance of shallow composite steel beams ($h \leq 500$ mm) is amplified somewhere between 60% to 80%.
 182 This should be carefully considered in the SCWB criterion. Vis-à-vis the above discussions, system-level tests (Suita et al
 183 2008) and supplemental system-level simulations (Lignos et al. 2013) suggest that when the slab contribution is disregarded,
 184 the prediction of soft-story collapse mechanisms due to potential drift concentration may be missed.

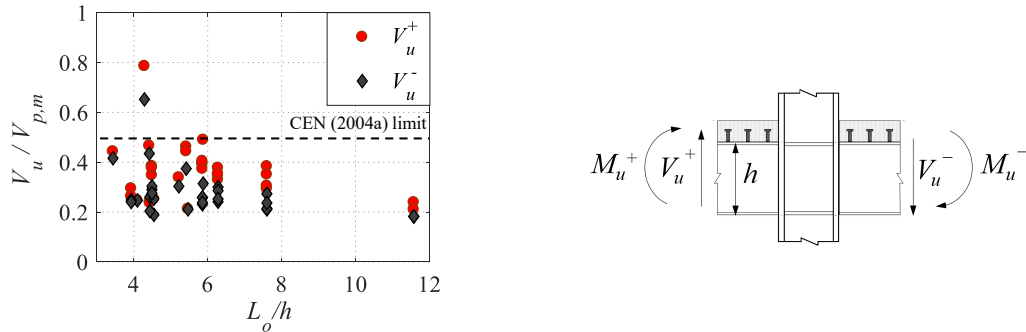
185 Referring to Fig. 4b, the sagging resistance of a beam increases when the degree of composite action, η increases. Due
 186 to brevity, the η values in Fig. 4b are only computed based on the European provisions (CEN 2004a, b). Note that η varies
 187 between codes due to differences in the recommended stud’s shear resistance and slab’s effective width. This issue is
 188 discussed later on in great detail. It is worth noting that deep steel MRF beams may require a large number of shear studs
 189 to develop a full composite action. However, a lesser number of shear studs is typically used in the actual design phase. In
 190 the context of the U.S. seismic provisions, a lower degree of composite action is actually desirable, considering that the
 191 AISC provisions (AISC 2016a) recommend that the SCWB ratio shall be just larger than 1.0.
 192



193
 194 **Fig. 4.** Dependence of the sagging resistance on the beam’s (a) depth, (b) the degree of composite action based on Eurocode
 195 provisions (CEN 2004a, b) and (c) span-to-depth ratio
 196

197 Figure 4c shows that composite steel beams with low L_o/h ratio (mainly deep beams) have a higher moment-shear
 198 interaction, which in turn decreases the beam’s attained sagging resistance. Notably, although a number of composite steel
 199 beams had a $L_o/h < 5$, only two specimens did not develop their bare steel plastic resistance $M_{p,e}$. This suggests that the L_o/h
 200 > 5 limit specified by ANSI/AISC 358-16 (AISC 2016c) for prequalified beam-to-column connections is rational. Fig. 5
 201 shows the maximum shear demand on the beam, V_u , with respect to L_o/h . The shear demand, V_u , is normalized with respect
 202 to the plastic shear resistance, $V_{p,m}$, of the bare steel beam, based on the measured yield stress. Albeit the shear demand on
 203 the beam under sagging becomes maximum, V_u values are plotted for both sagging and hogging bending (i.e., V_u^+ and V_u^- ,
 204 respectively). All but one specimen experienced a $V_u/V_{p,m}$ ratio less than 0.5. This implies that the moment-shear interaction
 205 was not relevant in most cases, which complies with the Eurocode seismic provisions. Ten beams experienced a $V_u/V_{p,m}$
 206 ratio larger than 0.4. These beams do not comply with the L_o/h prequalification limits of ANSI/ASCI 358-16 (AISC 2016c).
 207

This paper is published as : El Jisr, H., Elkady, A., Lignos, D.G. (2019). “Composite steel beam database for seismic design and performance assessment of composite-steel moment-resisting frame systems, Bulletin of Earthquake Engineerin, Vol. 17(6), pp. 3015-3039, doi: 10.1007/s10518-019-00564-w.



208 **Fig. 5.** Dependence of maximum shear demand-to-shear resistance ratio on the beam’s span-to-depth ratio

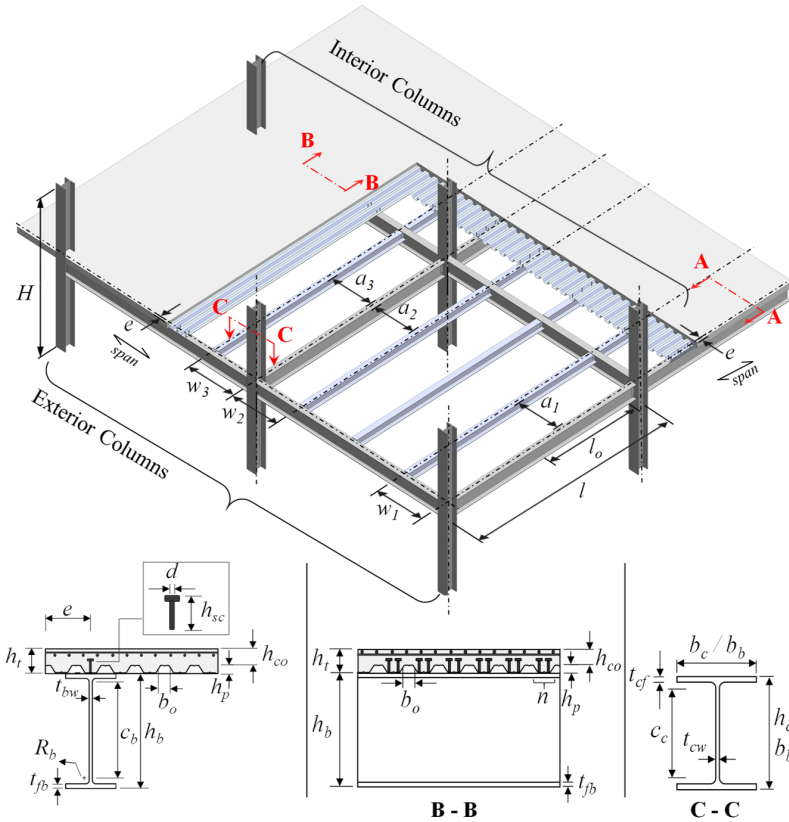
209
210 3.1.1. Assessment of the Code-Based Sagging Resistance of Composite Steel Beams

211
212 With respect to the design sagging resistance, discrepancies between the design codes are limited to (i) the assumed
213 effective width and compressive stress of the slab and (ii) the assumed shear stud resistance. In this context, a brief
214 discussion of these differences is provided below.

215
216 *Slab’s Effective Width and Compressive Stress*

217 An illustration of the basic dimensions used for effective width calculations by the three codes as well as a tabulated
218 comparison of the formulas used for these calculations are shown in Fig. 6a and 6b, respectively. The general consensus is
219 that the effective width calculation as per the U.S. and Japanese provisions is simpler than that of the European provisions.
220 For instance, the effective width according to the Eurocode provisions differs depending on (i) the loading condition
221 (gravity/seismic), (ii) the joint configuration (exterior/interior column), and (iii) the presence of transverse beams or
222 anchored rebar in the slab. The Japanese provisions simply recommend an effective width equal to the column flange width.
223 This agrees with past findings from Du Plessis and Daniels (1972) but it is a conservative assumption in most cases.

224 For the concrete slab’s design compressive stress, both the European (CEN 2004b) and American (AISC 2016b)
225 provisions consider 85% of the concrete specified/characteristic compressive strength. This value is rational for partially-
226 composite steel beams (Civjan et al. 2001; Cordova and Deierlein 2005). On the other hand, the Japanese provisions
227 consider twice the compressive strength for fully composite steel beams, in which the effective stress can reach up to $1.8f'_c$.
228 This is consistent with observations from past studies (Du Plessis and Daniels 1972; Tagawa et al. 1989).
229



Code	Effective width*	
	Interior column	Exterior column
CEN (2004a)	min $\left\{ \begin{array}{l} 0.075l \\ e \end{array} \right.$	⁽¹⁾ min $\left\{ \begin{array}{l} 0.075l \\ e \end{array} \right.$
		⁽²⁾ min $\left\{ \begin{array}{l} 0.5(b_b + 0.7h_c) \\ e \end{array} \right.$
		⁽³⁾ min $\left\{ \begin{array}{l} 0.5(b_b + 0.7h_c) \\ 0.05l \\ e \end{array} \right.$
AISC (2016a)	min $\left\{ \begin{array}{l} 0.0125l \\ w \\ e \end{array} \right.$	
AIJ (2010a)		b_b

* Effective width on each side of the beam web centerline
⁽¹⁾ Transverse beams with stud connectors and column strong axis oriented in loading direction. Concrete slab up to exterior face of column or beyond
⁽²⁾ Same as (1) but without steel transverse beams or steel transverse beams without stud connectors
⁽³⁾ All other layouts

230

231 **Fig. 6.** (a) Illustration of frame and composite steel beam dimensions for effective width computations; and (b) comparison
 232 of code-based effective width for plastic analysis
 233

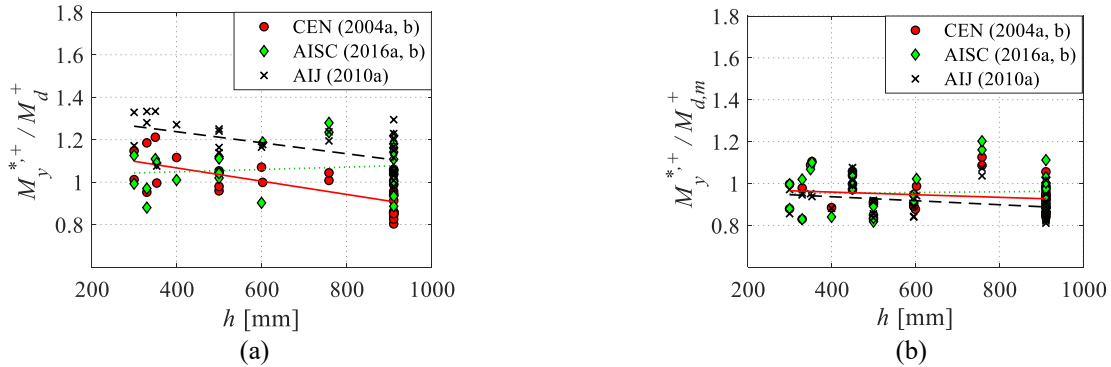
234 *Shear Resistance of Headed Studs*

235 Both Eurocode 4-Part 1 (CEN 2004b) and ANSI/AISC 360-16 (AISC 2016b) reduce the stud’s shear resistance in the
 236 presence of a steel deck, regardless of its orientation. The Japanese provisions (AIJ 2010a) only consider this reduction if
 237 the steel deck ribs are oriented perpendicular to the steel beam. In general, the reduction factor is a function of the deck and
 238 stud dimensions. If the steel deck is oriented perpendicular to the beam, this factor becomes also dependent on the number
 239 of studs per rib. The U.S. (AISC 2016a) and European (CEN 2004a) provisions require an additional 25% reduction on the
 240 shear resistance of headed studs in seismic load resistant systems.
 241

242 *Comparison of Code-based and Test-based Sagging Resistances*

243 The design sagging resistance, M_d^+ , is calculated here using plastic analysis as adopted in the three considered design
 244 provisions. Figure 7a shows the ratios of test- to code-based sagging resistance, $M_y^{*,+}/M_d^+$, versus the beam depth. The trend
 245 lines suggest that the Eurocode tends to overestimate the sagging resistance of deep beams ($h \approx 900$ mm). This is due to the
 246 assumed constant material overstrength factor of 1.25, regardless of the steel material type. The collected deep beams are
 247 mainly made of A992 Gr.50 steel. This has a lower material overstrength ($R_y = 1.1$). This issue as well as the observed
 248 variability in the M_d^+ values diminish between the three codes when the measured yield stress is used to calculate the design
 249 sagging resistance, $M_{d,m}^+$ (see Fig. 7b). Thus, the material overstrength shall be related to the steel grade (refer to Fig. 2) as
 250 adopted in ANSI/AISC 341-16 (AISC 2016a). In a similar manner, the proposed material overstrength values from the
 251 OPUS program (Braconi et al. 2013) can be adopted in future editions of Eurocode 8. It is also worth noting that the Japanese
 252 steel industry addressed this issue by developing new steel grades with specified upper and lower limits on the yield stress
 253 (Nakashima et al. 2000; Kanno 2016).

254 The findings also suggest that the sagging resistance is not sensitive to the rest of the aforementioned differences between
 255 design codes. Therefore, the ANSI/AISC approach (AISC 2016a, b) is recommended for the computation of the stud’s shear
 256 resistance given its simpler formulation. Since the sensitivity of the results to variations in the slab’s effective width is also
 257 negligible, the detailed approach of Eurocode 8-Part 1 (CEN 2004a) is not justifiable. Alternatively, either the AISC (2016a,
 258 b) or the AIJ (2010a) approaches are recommended for future revisions of Eurocode 8-Part 1.
 259

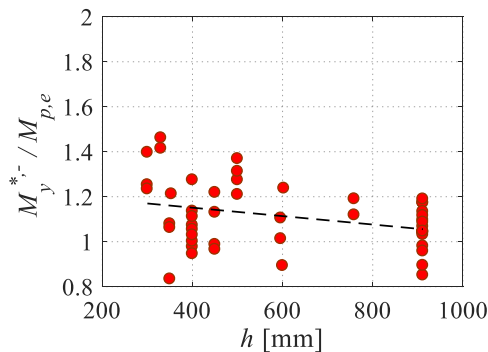


260 **Fig. 7.** Test- to code-based sagging resistance ratio versus beam depth based on (a) expected material properties according
 261 to respective code; and (b) measured material properties
 262

263 3.2. Hogging Resistance

264
 265 Fig. 8 shows the ratio of the test-based hogging resistance to the expected bare steel beam plastic resistance ($M_p^{*,-} / M_{p,e}$)
 266 versus the beam depth. The test-based hogging resistance is, on average, 10% higher than $M_{p,e}$. This is consistent with prior
 267 observations by Elkady and Lignos (2014). This amplification is attributed to contributions from the slab longitudinal
 268 reinforcement and the metal deck. This becomes more evident in shallow beams. Note that the majority of the collected
 269 tests includes reinforced slabs with a steel wire mesh (reinforcement area less than 5 mm²/cm slab width). Interestingly,
 270 shallow beams ($h = 300 \sim 330$ mm) with relatively high deck reinforcement (8~13 mm²/cm), that were tested by Bursi and
 271 Gramola (2000) and Kishiki et al. (2010), developed the largest amplification factors of 1.4 to 1.5 as highlighted in Fig. 8.
 272

273 Most of the collected reports did not indicate the exact location of the slab reinforcement including their measured yield
 274 stress. Therefore, it was possible to calculate the design hogging resistance, $M_{d,m}^-$ for only eight of the collected specimens.
 275 The ANSI/AISC 360-16 (AISC 2016b) allows for the consideration of the slab reinforcement within the sagging plastic
 276 effective width (see Fig. 4b) while the Eurocode 8 (CEN 2004a) distinguishes between the effective width under sagging
 277 and hogging bending. However, the average ratio, $M_y^{*,-} / M_{d,m}^-$, is found to be 0.97 and 0.96 for the AISC (2016a, b) and
 278 Eurocode (CEN 2004a, b), respectively. This implies that the sensitivity of the hogging resistance to the slab effective width
 279 variation is negligible. Therefore, it is rational to adopt the simpler ANSI/AISC 360-16 (AISC 2016b) approach for the
 280 effective width computations in future editions of Eurocode 8-Part 1.



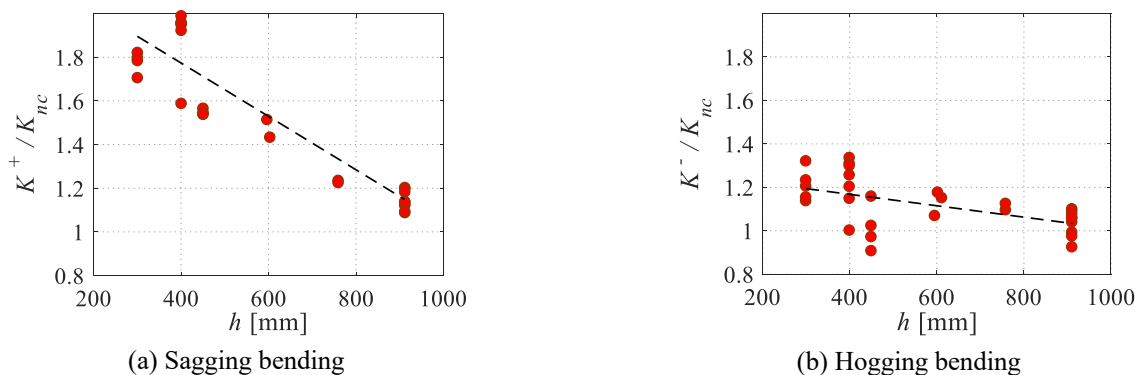
281 **Fig. 8.** Normalized test-based hogging resistance versus beam depth

282 3.3. Effective Stiffness

283

284 The effective stiffness under sagging (K^+) and hogging (K^-) bending is plotted versus the beam depth in Fig. 9a and 9b,
 285 respectively. In this figure, the test-based stiffness is normalized by the theoretical stiffness of the non-composite steel
 286 beam, K_{nc} , considering both flexural and shear deformations. The test-based effective stiffness could only be obtained for
 287 29 specimens; those are the ones where the beam’s moment-rotation relation could be deduced from the reported test data.

288 Fig. 9a shows that the composite action amplifies the effective stiffness of shallow beams ($h \leq 500$ mm) under sagging
 289 bending by up to 100%. This agrees with findings from system-level experiments (Nakashima et al. 2007; Nam and Kasai
 290 2012). For deep beams ($h > 500$ mm), the effective stiffness increases, on average, by 30%. Referring to Fig. 9b, the effective
 291 stiffness under hogging bending is amplified by up to 35% depending on the beam depth and the amount of slab
 292 reinforcement as discussed earlier. For few specimens, the K^-/K_{nc} values are slightly less than 1.0, which is attributed to the
 293 sensitivity of K^- deduction from the test data. The effective stiffness is also dependent on the degree of composite action as
 294 discussed in the subsequent section.
 295



296 **Fig. 9.** Dependence of the composite steel beam’s effective stiffness on its depth

297
 298 3.3.1. Assessment of Code-based Effective Stiffness under Sagging Bending
 299

300 The three codes calculate the effective stiffness under sagging bending, based on the effective moment of inertia of the un-
 301 cracked fully-composite cross-section. The level of accuracy of these code estimates, that generally involve design-related
 302 reduction factors depending on a target limit state, is assessed here based on the deduced (i.e., actual) stiffness measurements
 303 of the collected test data (see Fig. 3). Section C-13 commentary of the ANSI/AISC 360-16 (AISC 2016b) as well as the
 304 Japanese (AIJ 2010a) provisions employ Eq. (2) to estimate the moment of inertia for partially-composite steel beams, I_{pc} ,
 305 in which, I_{nc} , and I_c are the moments of inertia of the non-composite and fully composite steel beams, respectively.
 306

$$307 \quad I_{pc} = I_{nc} + \sqrt{\eta}(I_c - I_{nc}) \quad (2)$$

308
 309 The ANSI/AISC 360-16 (AISC 2016b) recommends an additional 25% reduction in the composite beam’s moment of
 310 inertia for realistic deflection calculations (Leon 1990; Leon and Alsamsam 1993). For the same purpose, the Japanese
 311 provisions (AIJ 2010a) use a larger modular ratio, $n = 15$ (defined as the ratio of the steel-to-concrete elastic modulus).
 312 Based on Eq. (2), the effective moment of inertia depends on the assumed slab effective width, which in turn differs in the
 313 elastic and plastic ranges. In the former, the effective width is related to the shear lag phenomenon (Castro et al. 2007). In
 314 the latter, stress redistribution in the slab occurs due to material nonlinearity, which increases the corresponding slab
 315 effective width. Accordingly, different effective widths shall be assumed for the plastic flexural resistance and the
 316 serviceability calculations (stiffness and deflection checks). Table 2 summarizes a comparison of the effective widths
 317 proposed by the three design codes for elastic analysis. In summary, Eurocode 8 considers a smaller slab effective width
 318 for elastic analysis than for plastic flexural resistance calculations. The effective width, as per Eurocode 8, is also dependent
 319 on the column configuration as well as the presence of transverse beams and anchored rebar in the slab (CEN 2004a). The
 320 ANSI/AISC 360-16 (AISC 2016b) provisions do not distinguish between elastic and inelastic analysis. The Japanese design
 321 recommendations propose a different effective width for elastic analysis that depends on the beam span. Both Eurocode 8
 322 and Japanese provisions propose a fixed value for the modular ratio, n .

323 Figure 10 shows the ratio of the test- to code-based effective stiffness under sagging bending, K^+/K_d^+ versus the beam
 324 depth and degree of composite action. It appears that the 25% reduction imposed on I_{pc} by AISC (2016a, b) for realistic

This paper is published as : El Jisr, H., Elkady, A., Lignos, D.G. (2019). “Composite steel beam database for seismic design and performance assessment of composite-steel moment-resisting frame systems, Bulletin of Earthquake Engineering, Vol. 17(6), pp. 3015-3039, doi: 10.1007/s10518-019-00564-w.

325 deflection calculations results in a conservative estimate of the effective stiffness. However, long term effects, may actually
 326 reduce the effective stiffness of composite steel beams over a building’s life-cycle. This effect cannot be assessed here since,
 327 in most cases, the collected tests were conducted within one month after concrete casting.

Table 2. Summary comparison of code-based effective width computation for elastic analysis

Code	Effective width*		Modular ratio, n
	Interior column	Exterior column	
CEN (2004a)	$\min \left\{ \begin{array}{l} 0.0375l \\ e \end{array} \right.$	$^{(1)} \min \left\{ \begin{array}{l} 0.0375l \\ e \end{array} \right. \quad ^{(2)} \min \left\{ \begin{array}{l} 0.025l \\ e \end{array} \right.$	7
AISC (2016b)	$\min \left\{ \begin{array}{l} 0.0125l \\ w \\ e \end{array} \right.$		E_s / E_c
AIJ (2010b)	$\min \left\{ \begin{array}{ll} b + (0.5 - 0.6a/l)a & \text{if } a < 0.5l \\ b + 0.1l & \text{if } a \geq 0.5l \end{array} \right.$		15

* Effective width on each side of the beam web centerline b = Flange width/2 for symmetric slab configuration.
 (1) With transverse beams and anchored rebars = Flange width for asymmetric slab configuration.
 (2) Without transverse beams or rebars not anchored

330 In brief, the Eurocode and Japanese provisions provide close estimates of the effective stiffness with an average K^+ / K_d^+
 331 values of 0.96 and 0.91, respectively. The associated coefficient of variation (COV) is 0.12 and 0.06 for the Eurocode and
 332 Japanese data points, respectively. The higher dispersion based on the Eurocode is attributed to the fact that it always
 333 assumes a fully composite cross-section; thus the Eurocode is conservative for beams with lower degree of composite action
 334 ($K^+ / K_d^+ < 0.85$, see Fig. 10b) as well as for fully-composite shallow beams ($K^+ / K_d^+ > 1$).
 335
 336

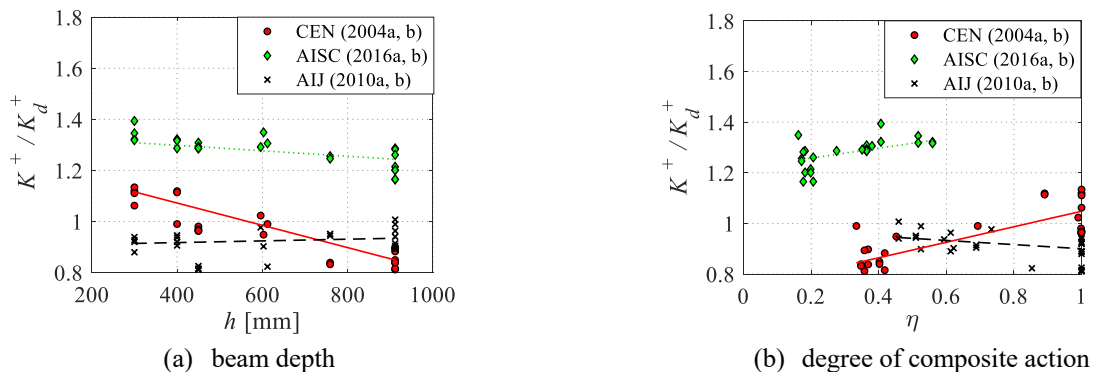


Fig. 10. Ratio of test- to code-based sagging effective stiffness

3.4. Plastic Rotation Capacity of Composite Steel Beams

341 The assembled database is used to quantify the pre- and post-capping plastic rotation capacities of composite steel
 342 beams, under sagging and hogging bending and to propose empirical equations for predicting these quantities. These
 343 equations can be used in the context of seismic assessment guidelines for new and existing steel frame buildings.

344 Eurocode 8-Part 3 (CEN 2005a) simply predicts a plastic rotation ($\theta_{p,pred}$) equal to $8\theta_y$ and $3\theta_y$ for Class 1 and 2 cross-
 345 sections, respectively (where θ_y is the chord rotation at yielding) for non-composite steel beams. These values are anchored
 346 to the near-collapse limit state (Panagiotakos and Fardis 2001), which corresponds to the plastic rotation capacity at 20%
 347 drop in the beam’s peak flexural resistance.

348 Using experimental data collected by Lignos and Krawinkler (2011, 2013), Hartloper and Lignos (2017) developed
 349 empirical equations to predict the pre- and post-capping plastic rotation of non-composite beams based on their first cycle
 350 envelope curve as defined in Fig. 3b. These equations are further refined here by supplementing the collected experiments

This paper is published as : El Jisr, H., Elkady, A., Lignos, D.G. (2019). “Composite steel beam database for seismic design and performance assessment of composite-steel moment-resisting frame systems, Bulletin of Earthquake Engineering, Vol. 17(6), pp. 3015-3039, doi: 10.1007/s10518-019-00564-w.

with data from non-composite steel beams that were conducted mostly in Europe. The equations are developed through standard multiple regression analysis (Chatterjee and Hadi 2015). The refined expressions are provided for θ_p^* and θ_{pc}^* as defined in Fig. 3. In particular, for standard non-composite steel non-RBS beams,

$$\theta_p^* = 0.25 \cdot \left(\frac{c}{t_w}\right)^{-0.9} \cdot \left(\frac{b}{2t_f}\right)^{-1.1} \cdot \left(\frac{L_b}{i_z}\right)^{-0.2} \cdot \left(\frac{L_o}{h}\right)^{1.1} \cdot \left(\frac{E}{f_{y,e}}\right)^{0.2} \quad (COV = 0.38) \quad (3)$$

$$\theta_{pc}^* = 12.67 \cdot \left(\frac{c}{t_w}\right)^{-0.9} \cdot \left(\frac{b}{2t_f}\right)^{-0.9} \cdot \left(\frac{L_b}{i_z}\right)^{-0.5} \cdot \left(\frac{E}{f_{y,e}}\right)^{0.1} \quad (COV = 0.44) \quad (4)$$

and for non-composite steel beams with RBS,

$$\theta_p^* = 0.12 \cdot \left(\frac{c}{t_w}\right)^{-0.5} \cdot \left(\frac{b}{2t_f}\right)^{-0.7} \cdot \left(\frac{L_b}{i_z}\right)^{-0.5} \cdot \left(\frac{L_o}{h}\right)^{0.8} \cdot \left(\frac{E}{f_{y,e}}\right)^{0.23} \quad (COV = 0.42) \quad (5)$$

$$\theta_{pc}^* = 4.91 \cdot \left(\frac{c}{t_w}\right)^{-1.1} \cdot \left(\frac{b}{2t_f}\right)^{-0.1} \cdot \left(\frac{L_b}{i_z}\right)^{-0.1} \cdot \left(\frac{E}{f_{y,e}}\right)^{0.09} \quad (COV = 0.47) \quad (6)$$

In which, L_b is the unbraced length of the beam, i_z is the weak-axis' radius of gyration, E and $f_{y,e}$ are the steel's modulus of elasticity and expected yield stress, respectively. The above equations are valid within the following ranges: $35 \leq c/t_w \leq 55$, $3 \leq b/2t_f \leq 8$, $20 \leq L_b/i_z \leq 80$ (RBS: $20 \leq L_b/i_z \leq 60$), $3 \leq L_o/h \leq 8$ (RBS: $5 \leq L_o/h \leq 8$), $440 \leq E/f_{y,e} \leq 830$.

To assess the predicted plastic rotation capacities based on the proposed Eqs. (3) to (6) as well as the Eurocode 8 approach, the pre- and post-capping plastic rotations under sagging and hogging bending are deduced from the gathered experimental data. To be consistent with the Eurocode 8 definition, the plastic rotation at 20% drop in peak flexural resistance, $\theta_{p,80\%M_u}^{*+/-}$, is deduced from the test data. The same is done to deduce the predicted plastic rotation capacities corresponding to 80% $M_u^{+/-}$ based on Eqs. (3) to (6). In particular, $\theta_{p,pred} = \theta_p^{*+/-} + 0.2 \theta_{pc}^{*+/-}$. The ratio of test-based to predicted plastic rotation, $\theta_{p,80\%M_u}^{*+/-} / \theta_{p,pred}$, ratio versus the beam's web slenderness ratio (c/t_w) is plotted in Fig. 11. The web slenderness ratio is used here since steel beams in fully restrained beam-to-column connections are mainly prone to web local buckling followed by flange buckling (Lignos and Krawinkler 2011). Also note that data points in this figure exclude tests where beams experienced premature fracture or those terminated prior to reaching 80% M_u .

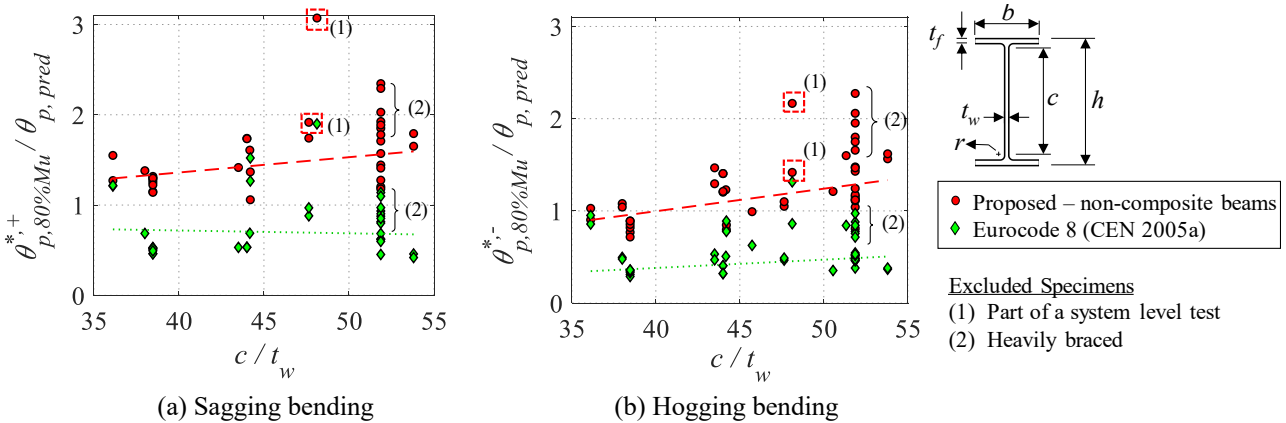


Fig. 11. Ratio of test-based to predicted plastic rotation at 20% flexural strength loss with respect to beam's web slenderness

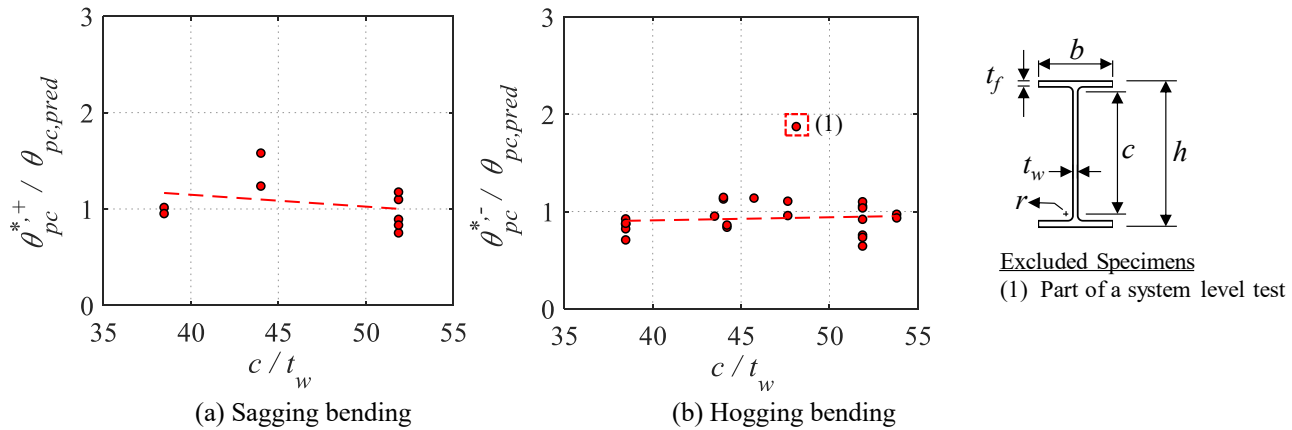
Referring to Fig 11a and 11b, the plastic rotation capacity under sagging bending is generally larger than that under hogging bending. This is due to the lateral restraint provided by the slab to the steel beam's top flange and top portion of the web, thereby delaying the top flange local buckling. Moreover, Eurocode 8-Part 3 consistently overestimates the plastic rotation capacity under both sagging and hogging bending by about 50%, regardless of the c/t_w and degree of composite action, η . This agrees with prior related studies (Araújo et al. 2017). The main reason is that this approach ignores the influence of geometric and material properties of a steel beam on its plastic rotation capacity. Referring to Fig. 11b, for

This paper is published as : El Jisr, H., Elkady, A., Lignos, D.G. (2019). “Composite steel beam database for seismic design and performance assessment of composite-steel moment-resisting frame systems, Bulletin of Earthquake Engineering, Vol. 17(6), pp. 3015-3039, doi: 10.1007/s10518-019-00564-w.

387 hogging bending, the plastic rotation predicted based on Eqs. (3) to (6) matches the measured one relatively well. Under
 388 sagging bending, the refined equations underestimate $\theta_{p,80\%M_u}^{*+}$ by almost a constant value of 1.5. This is expected since
 389 these equations are meant for non-composite beams. The scatter around the predicted plastic rotation values at $c/t_w \approx 52$ is
 390 attributed to differences in lateral stability bracing between the collected tests. In fact, several of the collected specimens
 391 were heavily braced such that the predominant instability would be cross-sectional local buckling. Based on these
 392 observations, for composite steel beams under sagging bending, $\theta_{p,80\%M_u}^{*+} = 1.5 \theta_{p,pred}$ as per Eqs. (3) to (6) depending on the
 393 beam-to-column connection type. Similarly, under hogging bending, $\theta_{p,80\%M_u}^{*-} = \theta_{p,pred}$.

394 Interestingly, one test specimen (highlighted in Fig. 11) achieved a much larger $\theta_{p,80\%M_u}^{*+/-}$ of 7.8% and 5.5% rad under
 395 sagging and hogging bending, respectively. This corresponds to an interior beam as part of a system-level test (Del Carpio
 396 et al. 2014). Cordova and Deierlein (2005) found that the axial restraint provided by the slab continuity in composite steel
 397 concrete MRFs increases the plastic rotation capacity of interior joint beams. This is not captured in the majority of the
 398 available experimental data due to their simplified boundary conditions (Roeder 2000). The authors are currently
 399 investigating this issue more thoroughly in a separate study.

400 The post-capping plastic rotation is deduced from 13 and 25 tests under sagging and hogging bending, respectively. The
 401 deduced $\theta_{pc}^{*+/-}$ values are normalized with respect to the post-capping rotation predicted by Eqs. (4) and (6) and plotted
 402 versus c/t_w in Fig. 12. Note that Eurocode 8-Part 3 does not provide estimates for this quantity. The data trends suggest that
 403 the influence of the concrete slab on the post-capping plastic rotation is not as pronounced as on $\theta_{p,80\%M_u}^{*+/-}$. This agrees with
 404 prior findings by Elkady and Lignos (2014). Under sagging bending, the post-capping plastic rotation is about 20% larger
 405 than that predicted for the non-composite beam (see Fig. 12a). Under hogging bending (see Fig.12b), θ_{pc}^{*-} is, on average,
 406 10% lower than that predicted by the regression equations for non-composite steel beams. Under hogging bending, a bigger
 407 portion of the steel cross-section is under compression, which increases the potential for local and/or lateral torsional
 408 buckling (PEER/ATC 2010). In conclusion, it is recommended that for composite steel beams under sagging bending, the
 409 post-capping plastic rotation shall be taken as 1.2 times θ_{pc}^* of non-composite beams as per Eqs. (4) and (6). Under hogging
 410 bending, the post-capping plastic rotation shall be computed directly from Eqs. (4) and (6).
 411



412 **Fig. 12.** Ratio of test-based to predicted post-capping plastic rotation with respect to the beam's web slenderness
 413

414 **4. Influence of Composite Action on Beam-to-Column Web Panel Zone**

415
 416 The shear demand on the beam-to-column web panel zone of 45 composite steel beams is deduced and assessed with
 417 respect to the web panel shear resistance computed by the American, European and Japanese steel design specifications
 418 (CEN 2005c; AIJ 2010a; AISC 2016b). Referring to Fig. 13, based on the equilibrium of the external forces at a given joint,
 419 the maximum shear demand on the panel zone, $V_{PZ,demand}$, is deduced from the tests as follows,
 420

$$421 \quad V_{PZ,demand} = \frac{M_u^+}{d_{eff}^+} + \frac{M_u^-}{d_{eff}^-} - V_{col} = \frac{M_u^+}{d_{eff}^+} + \frac{M_u^-}{d_{eff}^-} - \frac{M_u^+ + M_u^-}{H} \cdot \frac{l}{l - h_c} \quad (7)$$

422

in which, M_u^+ and M_u^- are the peak sagging and hogging bending demands at the column face, respectively, d_{eff}^+ and d_{eff}^- are the effective panel zone depths for sagging and hogging bending, V_{col} is the shear force in the column, l and H are defined in Fig. 6a. Note that M^- is zero for exterior joints. Under hogging bending, the effective depth d_{eff}^- is equal to the bare steel beam depth, h . Under sagging bending, the top flange resultant force shifts towards the slab and the resulting d_{eff}^+ is deduced by Eq. (8) that considers the concrete slab geometry (Kim and Engelhardt 2002; Elkady and Lignos 2014),

$$d_{eff}^+ = h + h_t - 0.5h_c - 0.5t_{bf} \quad (8)$$

Generally, the yield shear resistance of the panel zone, V_y , is expressed by Eq. (9), in which A_v is the shear area of the panel zone, f_{yv} is the shear yield stress (taken as $0.58 \sim 0.6f_{y,n}$), and α is a reduction factor that accounts for the axial load-shear interaction. In the American and Japanese provisions, α depends on the column axial load demand. The axial force-shear interaction is ignored in Eurocode 3 (CEN 2005c). Instead, a flat reduction factor equal to 0.9 is considered. Ciutina and Dubina (2003) stated that this factor accounts for the reduction due to axial load-shear interaction.

$$V_y = \alpha A_v f_{yv} \quad (9)$$

Eurocode 8 allows up to 30% contribution of the panel zone to the joint's total inelastic deformation. The panel zone plastic shear resistance is expressed by Eq. (10) as per ANSI/AISC 360-16 (AISC 2016b) and Eq. (11) as per Eurocode 3, in which, b_c and t_{cf} are the width and thickness of the column flange, respectively; h_b and t_{bf} are the beam's depth and flange thickness, respectively (see Fig. 13). The Japanese code reduces the shear demand by 25%. The joint is then designed for V_y (Nakashima et al. 2000).

$$V_p = V_y \left(1 + 3 \frac{b_c t_{cf}^2}{h_b h_c t_p}\right) \quad (10)$$

$$V_p = V_y + \frac{b_c t_{cf}^2}{(h_b - 2t_{bf})} f_{y,n} \quad (11)$$

None of the three design provisions suggests how the composite slab shall be considered in the panel zone shear demand and resistance computations. The panel zone's yield and plastic shear resistances are calculated based on the three code provisions based on nominal material properties.

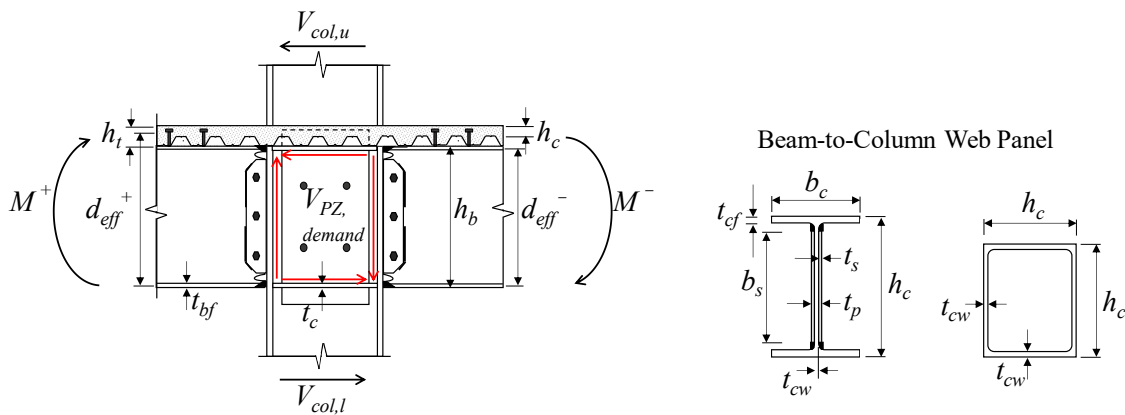


Fig. 13. Panel zone dimensions and definition of the effective depth under sagging and hogging bending

Figure 14a and 14b show the panel zone shear resistance, $V_{PZ,d}$, versus the panel zone shear demand, $V_{PZ,demand}$, for wide-flange and hollow structural section (HSS) columns, respectively. For reference, three dashed lines are superimposed in Fig. 14 that represent a $V_{PZ,d}$ to $V_{PZ,demand}$ ratio of 0.6, 1.0 and 1.67. Also in Fig. 14a, the labeled specimens were intentionally designed for a very strong ('S') or very weak ('W') panel zone. The figure shows that the estimated yield shear resistance based on AISC (2016b) and AIJ (2010a) is between 0.70 to 1.25 times the panel zone shear demand. In total, 14 out of 23

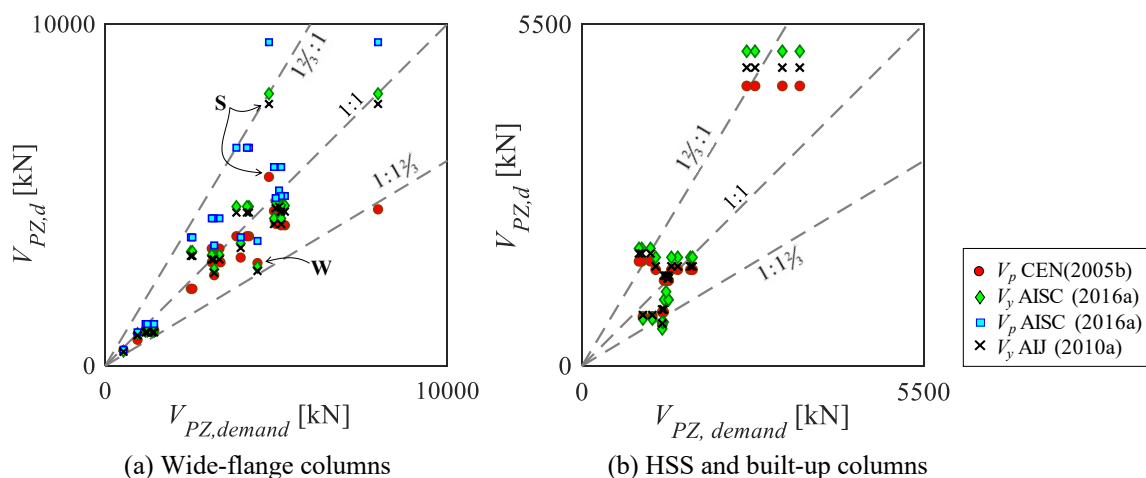
This paper is published as : El Jisr, H., Elkady, A., Lignos, D.G. (2019). “Composite steel beam database for seismic design and performance assessment of composite-steel moment-resisting frame systems, Bulletin of Earthquake Engineering, Vol. 17(6), pp. 3015-3039, doi: 10.1007/s10518-019-00564-w.

458 wide-flange specimens experienced a shear demand greater than the yield resistance because the amplified sagging flexural
 459 resistance of the composite beam was neglected in design; hence underestimating the shear demand.

460 The estimated panel zone shear resistance according to Eurocode 3 varied between 0.6 to 1.1 times the corresponding
 461 shear demand. The Eurocode approach is particularly conservative for panel zones with doubler plates. This is because i)
 462 the Eurocode only considers a single doubler plate thickness even if two plates exist and ii) the panel zone shear resistance
 463 includes a 0.9 reduction factor regardless of the imposed axial load demand. All but two specimens experienced a shear
 464 demand greater than the Eurocode-based panel zone shear resistance. This conservatism is due to the associated uncertainty
 465 in estimating the panel zone contribution to the plastic rotation demands of the beam-to-column joint (Castro et al. 2008).

466 Referring to Fig. 14b, about half of the specimens with HSS and built-up box sections experienced a lower demand than
 467 the panel zone shear resistance, regardless of the respective code provision. Specimens in which the demand was higher
 468 than the code-based yield shear resistance experienced panel zone shear yielding (see Table 3). According to Nakashima et
 469 al. (2000), while Japanese limit state design principles encourage panel zone yielding, Japanese buildings are less commonly
 470 controlled by panel zone yielding.

471



472 **Fig. 14.** Code-based panel zone shear resistance versus maximum panel zone shear demand

473

474 The gathered experimental data suggest that story drift demands exceeding 5% can be sustained even if the panel zone
 475 develops a total shear distortion up to 10 γ_y (≈ 0.023 rad). This can be achieved with a $V_{PZ,d} / V_{pl,b}$ ratio of 0.8. The limit,
 476 which is applicable to all three design provisions, is based on the panel zone’s yield shear resistance and the plastic flexural
 477 resistance of composite steel beams. Because this finding is based on subassembly test data, system-level studies shall be
 478 conducted in order to evaluate the influence of controlled inelastic behavior of panel zones on the dynamic response of steel
 479 MRFs relative to “strong” panel zone designs. However, this is outside the scope of the present work.

480

481 4.1 Recommendations for Panel Zone Shear Resistance

482

483 While design provisions allow for controlled inelastic panel zone yielding, there is no clear guidance on the relative
 484 panel zone-to-beam shear resistance. For this purpose, specimens for which the panel zone yield deformation was reported
 485 are analyzed separately. The collected specimens are summarized in Table 3 along with their reported failure mode.
 486 Specimens that fractured prior to a peak story-drift ratio of 5% and those that do not reflect the current design practice
 487 according to modern design provisions, are listed in Table 3 but are excluded from the subsequent assessment.

488 Figure 15 shows the panel zone shear resistance, $V_{PZ,d}$, normalized by $V_{pl,b}$ versus the panel zone total rotation (expressed
 489 as multiples of the nominal yield rotation in shear, γ_y). The $V_{pl,b}$ is the shear demand on the panel zone due to the development
 490 of the composite beam’s plastic flexural resistance. This is calculated according to the respective design provision using the
 491 measured material properties to eliminate the material uncertainty (i.e., M_{d,m^+} and M_{d,m^-} as defined earlier). This measure
 492 of the beam’s relative shear resistance has been adopted in prior related studies (Roeder 2002; Lee et al. 2005). Note that
 493 the calculated beam plastic shear resistance accounts for the presence of the slab and neglects cyclic hardening.

This paper is published as : El Jisr, H., Elkady, A., Lignos, D.G. (2019). “Composite steel beam database for seismic design and performance assessment of composite-steel moment-resisting frame systems, Bulletin of Earthquake Engineering, Vol. 17(6), pp. 3015-3039, doi: 10.1007/s10518-019-00564-w.

494 Referring to Fig. 15a, composite connections with wide-flange columns and a $V_{PZ,d}$ -to- $V_{pl,b}$ ratio larger than 0.8, attained
 495 a shear distortion angle of up to $10\gamma_y$ ($\gamma_y=0.023$ rad) without experiencing premature fracture. Lee et al. (2005) found that a
 496 $V_{PZ,d}$ -to- $V_{pl,b}$ ratio between 1.10 and 1.42 is sufficient for the panel zone to develop a plastic rotation of 0.01 rad. However,
 497 the influence of the composite slab was disregarded in this case. When the $V_{PZ,d}$ -to- $V_{pl,b}$ ratio is between 1.10 to 1.42, the
 498 panel zone develops a rotation of $8.5\gamma_y$; i.e., the plastic rotation is equal to 0.019 rad, which still exceeds 0.01 rad.

499 Referring to Fig. 15b, for HSS columns, only three data points were collected (Yamada et al. 2009, Kishiki et al. 2010).
 500 Although inconclusive, two of these specimens experienced a panel zone shear distortion more than $15\gamma_y$. Those were
 501 through-diaphragm connections with fully-composite shallow beams. The specimen tested Kishiki et al. (2010) had a fully
 502 composite beam with a solid slab. Consequently, the composite beam remained elastic due to the large amplification in the
 503 plastic bending resistance and the plastic deformations of the subassembly were mainly concentrated in the panel zone.
 504
 505
 506

Table 3. Composite steel beam specimens with reported panel zone shear distortion

Reference	Specimen ID	Column section	$\frac{\gamma}{\gamma_y}$	Failure Mode	SDR_{max} [%]
Zhang et al. (2004)	SPEC-1	W36x230	4.91	Fracture in RBS bottom flange	5.0
	SPEC-2	W27x194	8.28	Fracture in RBS top flange	5.0
	SPEC-3	W27x194	4.64	Fracture in RBS	5.0
	SPEC-4	W36x150	5.78	Low cycle fatigue cracks	5.0
	SPEC-5	W27x146	7.93	Low cycle fatigue cracks	5.0
Ricles et al. (2000)	C5 ^(a)	W14x398	6.67	Fracture in top flange at shear stud in plastic hinge region	2.6 ^(b)
Engelhardt et al. (2000)	DBBWC	W14x398	7.8	Fracture at beam groove weld	6.0
	DBWWC	W14x398	8.40	Ductile tearing through top beam flange	7.0
	DBBWSPZC	W14x398	1.10	No fracture; test terminated	7.0
	DBWWPZC ^(a)	W14x283	23.23	Fracture in beam flange weld and shear-tab-to-column weld	7.0
Uang et al. (2004)	NIST-2C ^(a)	W14x426	2.58	No fracture; test terminated	4.0
Yamada et al. (2009)	Beam 1	HSS300x300x9	18.15	No fracture; test terminated	9.0
	Beam 2 ^(a)	HSS300x300x9	3.60	Beam fracture at scallop location	2.5
Kishiki et al. (2010)	F_Full	HSS250x250x9	22.07	No fracture; test terminated	5.0
	D_LS	HSS250x250x12	5.19	No fracture; test terminated	5.0
	D_SS ^(a)	HSS250x250x12	4.84	Beam fracture	3.5
Sumner & Murray (2002)	4E-1.25-1.375-24	W14x257	1.83	Bolt tension rupture	5.0
Kim & Lee (2017)	PN500-C ^(a)	H400x400x13x21	15.17	Fatigue fracture in bottom flange weld	4.0 ^(b)
	PN500C-HST ^(a)	H400x400x13x21	28.56	Low cycle fatigue beam fracture	7.0 ^(b)
	PN500C-SH	H400x400x13x21	5.42	No fracture	>5.0 ^(b)
	PN500C-TH	H400x400x13x21	9.07	No fracture	>5.0 ^(b)
Del Carpio et al. (2014)	RBS-A	W12x30	3.81	No fracture; test terminated	16.4

^(a) Specimens that are excluded from subsequent discussion

^(b) Total plastic rotation reported instead of story drift ratio

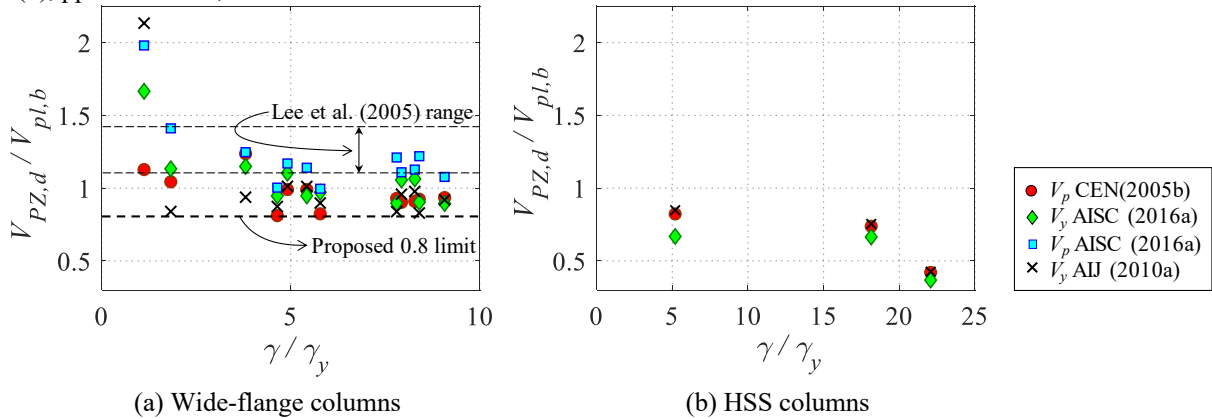


Fig. 15. Relative panel-zone-to-beam shear resistance against the normalized panel zone's distortion angle

509
510
511
512
513
514
515
516
517
518
519
520
521
522
523
524
525
526
527
528
529
530
531
532
533
534
535
536
537
538
539
540
541
542
543
544
545
546
547

5. Conclusions

This paper investigates the composite steel beam effects on the seismic design and performance assessment of composite-steel moment resisting frames (MRFs). For this purpose, a publicly available database of 97 composite steel beams was assembled. Several parameters were investigated including the sagging and hogging flexural resistances, the effective stiffness and the plastic rotation capacity of composite steel beams. The influence of the slab on the beam-to-column web panel shear resistance was also investigated. A comparison between the European, American and Japanese provisions was conducted; the aim of which is to provide design recommendations on how to properly consider the composite action in future design code revisions. Empirical formulations were also developed that capture the asymmetric behavior of composite steel beams under cyclic loading. Such relationships can be used in seismic assessment of new and existing steel frame buildings based on nonlinear static (pushover) analysis. The main findings are as follows:

- The sensitivity of the results to discrepancies between the three evaluated design provisions with regards to the computation of the sagging flexural resistance, $M_y^{*,+}$, is not significant. Therefore, the detailed approach presented in Eurocode 8-Part 1 (CEN 2004a) for calculating the slab effective width is not justified. Instead, this approach should be replaced with a simpler one (e.g., ANSI/AISC 360-16 AISC 2016b).
- The sagging flexural resistance, $M_y^{*,+}$, of shallow composite steel beams ($h < 500$ mm) is at least 1.4 times larger than that of deep beams. This value may vary considerably depending on the corresponding degree of composite action. In low rise steel frame buildings and/or steel buildings with space steel MRFs in which the degree of composite action is at least 0.4, the strong-column/weak-beam ratio shall be based on a beam's sagging flexural resistance.
- The hogging flexural resistance, $M_y^{*, -}$, of a composite steel beam is, on average, 10% larger than the corresponding one of the bare steel beam. This is attributed to the slab longitudinal reinforcement and the metal deck. The hogging plastic flexural resistance of a composite steel beam is sensitive to the steel material overstrength. This is traced well based on the ANSI/AISC 341-16 (AISC 2016a) seismic provisions because expected material properties are employed depending on the corresponding steel material grade. It is recommended that the material overstrength factors developed within the OPUS program (Braconi et al. 2013) are adopted in future editions of Eurocode 8-Part 1.
- Shallow composite steel beams ($h \leq 500$ mm) under sagging bending have an equivalent flexural stiffness of at least 1.6 times the effective flexural stiffness of the bare steel beam. This value decreases by up to 20% for deep composite steel beams ($h > 500$ mm). As such, the Eurocode (CEN 2004a, b) stiffness formulation exhibits higher dispersion because its estimation is not based on partially composite steel beams. Hence, the approaches discussed in the AISC and Japanese provisions are recommended for calculating the effective beam stiffness under sagging bending.
- The pre-capping plastic rotation capacity of composite steel beams is, on average, 50% higher than that of bare steel beams under sagging moment. When the beam is under hogging bending, the observed differences between composite and bare steel beams diminish. The Eurocode 8-Part 3 (CEN 2005a) formulations overestimate the measured plastic rotation capacities of steel beams in all the examined cases. This is attributed to the fact that the Eurocode approach does not consider the influence of the geometric and material properties of a steel beam on its plastic rotation capacity.

This paper is published as : El Jisr, H., Elkady, A., Lignos, D.G. (2019). “Composite steel beam database for seismic design and performance assessment of composite-steel moment-resisting frame systems, Bulletin of Earthquake Engineering, Vol. 17(6), pp. 3015-3039, doi: 10.1007/s10518-019-00564-w.

- 548 - The post-capping plastic rotation of composite steel beams is less sensitive to the presence of the slab. This is attributed
549 to the fact that in the post-peak response, the slab is typically cracked, thereby becoming less effective in delaying
550 local buckling-induced softening under cyclic loading.
- 551 - Empirical expressions are developed to reliably compute the plastic rotation capacity of composite steel beams. These
552 expressions can be directly used for the seismic assessment of new and existing steel MRF systems based on nonlinear
553 static analysis within the framework of Eurocode 8-Part 3 (CEN 2005a) and ASCE/SEI 41-17 (ASCE 2017). These
554 expressions effectively capture the dependencies of pre- and post-capping plastic rotation capacities of composite steel
555 beams with respect to the beam’s geometric and steel material properties.
- 556 - System-level tests suggest that the plastic rotation capacity of interior beam-to-column connections is at least 50%
557 larger than that of exterior joints due to the slab continuity that is not properly traced in typical beam-to-column
558 subassembly experiments. This deserves more attention in future studies and requires system-level physical testing.
- 559 - The panel zone shear yield resistance is nearly the same in the three design provisions that were evaluated. However,
560 Eurocode 3-Part 1-8 (CEN 2005c) is conservative if doubler plates exist on both sides of the column web. The reason
561 is that one of the two doubler plates is disregarded from the computation of the panel zone shear resistance.
- 562 - The panel zone in wide-flange steel columns may be designed such that the relative panel zone-to-beam shear
563 resistance, $V_{PZ,d} / V_{pl,b} = 0.8$. This value is based on composite steel beam test data for which at least a 5% peak story
564 drift ratio was attained. In these tests, the panel zones developed a total shear distortion up to about 10‰ without
565 experiencing pre-mature fracture within the corresponding beam-to-column connection.

566 6. Acknowledgments

567 This study is based on work supported by the Swiss National Science Foundation (Project No. 200021_169248). The
568 financial support is gratefully acknowledged. Any opinions expressed in the paper are those of the authors and do not
569 necessarily reflect the views of sponsors. The authors would like to sincerely thank Prof. Masayoshi Nakashima, Prof.
570 Tomohiro Matsumiya, Prof. Roberto Leon, Prof. Gregory G. Deierlein, Prof. Gilberto Mosqueda, Dr. Paul Cordova, and
571 Dr. Maikol Del Carpio for providing test data for the development of the composite steel beams database.

572 7. References

- 573 AIJ (2010a) Recommendation for limit state design of steel structures, 3rd edition. Architectural Institute of Japan
- 574 AIJ (2010b) Design recommendations for composite construction, 2nd edition. Architectural Institute of Japan
- 575 AISC (2016a) Seismic provisions for structural steel buildings, ANSI/AISC 341-16. American Institute for Steel
576 Construction, Chicago, IL
- 577 AISC (2016b) Specification for structural steel buildings, ANSI/AISC 360-16. American Institute for Steel Construction,
578 Chicago, IL
- 579 AISC (2016c) Prequalified connections for special and intermediate steel moment frames for seismic applications,
580 ANSI/AISC 358-16. American Institute for Steel Construction, Chicago, IL
- 581 Araújo M, Macedo L, Castro JM (2017) Evaluation of the rotation capacity limits of steel members defined in EC8-3. J
582 Constructional Steel Research 135:11–29. doi: 10.1016/j.jcsr.2017.04.004
- 583 Asada H, Matoba H, Tanaka T, Yamada S (2015) Retrofit effects for composite beams - Study on seismic retrofit of beam-
584 to-column connection using supplemental H-section haunches Part 2. J Struct Constr Eng AIJ 80:1479–1487
- 585 ASCE (2017) Seismic evaluation and retrofit of existing buildings: ASCE standard ASCE/SEI 41-17. American Society of
586 Civil Engineers, Reston, VA
- 587 Braconi A, Finetto M, Degee H, et al (2013) Optimising the seismic performance of steel and steel-concrete structures by
588 standardising material quality control (OPUS). European Commission, Luxembourg
- 589 Bursi O, Haller M, Lennon T, et al (2009) Prefabricated composite beam-to-column filled tube or partially reinforced-
590 concrete-encased column connections for severe seismic and fire loadings. European Commission, Luxembourg
- 591 Bursi OS, Gramola G (2000) Behaviour of composite substructures with full and partial shear connection under quasi-static
592 cyclic and pseudo-dynamic displacements. Mater Struct 33:154–163. doi: 10.1007/BF02479409
- 593 Castro JM, Dávila-Arbona FJ, Elghazouli AY (2008) Seismic design approaches for panel zones in steel moment frames. J
594 Earthq Eng 12:34–51. doi: 10.1080/13632460801922712

- This paper is published as :** El Jisr, H., Elkady, A., Lignos, D.G. (2019). “Composite steel beam database for seismic design and performance assessment of composite-steel moment-resisting frame systems, *Bulletin of Earthquake Engineering*, Vol. 17(6), pp. 3015-3039, doi: 10.1007/s10518-019-00564-w.
- 599 Castro JM, Elghazouli AY, Izzuddin BA (2007) Assessment of effective slab widths in composite beams. *J Constr Steel*
600 *Res* 63:1317–1327. doi: 10.1016/j.jcsr.2006.11.018
- 601 CEN (2004a) EN 1998-1: Eurocode 8: Design of structures for earthquake resistance – Part 1: General rules, seismic actions
602 and rules for buildings. European Committee for Standardization, Brussels, Belgium
- 603 CEN (2005a) EN 1998-3: Eurocode 8: Design of structures for earthquake resistance – Part 3: Assessment and retrofitting
604 of buildings. European Committee for Standardization, Brussels, Belgium
- 605 CEN (2005b) EN 1993-1-1: Eurocode 3: Design of steel structures – Part 1-1: General rules and rules for buildings.
606 European Committee for Standardization, Brussels, Belgium
- 607 CEN (2005c) EN 1993-1-8: Eurocode 3: Design of steel structures – Part 1-8: Design of joints. European Committee for
608 Standardization, Brussels, Belgium
- 609 CEN (2004b) EN 1994-1-1: Eurocode 4: Design of composite steel and concrete structures – Part 1-1: General rules and
610 rules for buildings. European Committee for Standardization, Brussels, Belgium
- 611 Chatterjee S, Hadi AS (2015) *Regression analysis by example*, 5th edition. John Wiley & Sons
- 612 Chen S-J, Chao YC (2001) Effect of composite action on seismic performance of steel moment connections with reduced
613 beam sections. *J Constr Steel Res* 57:417–434. doi: 10.1016/S0143-974X(00)00022-5
- 614 Cheng C-T, Chan C-F, Chung L-L (2007) Seismic behavior of steel beams and CFT column moment-resisting connections
615 with floor slabs. *J Constr Steel Res* 63:1479–1493. doi: 10.1016/j.jcsr.2007.01.014
- 616 Cheng C-T, Chen C-C (2005) Seismic behavior of steel beam and reinforced concrete column connections. *J Constr Steel*
617 *Res* 61:587–606. doi: 10.1016/j.jcsr.2004.09.003
- 618 Ciutina AL, Dubina D (2003) Influence of column web stiffening on the seismic behaviour of beam-to-column joints. In:
619 *Proceedings of Stessa*. pp 269–75
- 620 Civjan S, Engelhardt M, Gross J (2001) Slab effects in SMRF retrofit connection tests. *J Struct Eng* 127:230–237. doi:
621 10.1061/(ASCE)0733-9445(2001)127:3(230)
- 622 Cordova PP, Deierlein G (2005) Validation of the seismic performance of composite RCS frames: Full-scale testing,
623 analytical modeling, and seismic design. The John A. Blume Earthquake Engineering Center, Stanford University,
624 Stanford, CA
- 625 Del Carpio M, Mosqueda G, Lignos D (2014) Hybrid simulation of the seismic response of a steel moment frame building
626 structure through collapse. Multidisciplinary Center for Earthquake Engineering Research, University at Buffalo
- 627 Du Plessis DP, Daniels JH (1972) Strength of composite beam-to-column connections. Fritz Engineering Laboratory,
628 Lehigh University, Bethlehem, PA
- 629 Elkady A, Lignos DG (2014) Modeling of the composite action in fully restrained beam-to-column connections:
630 implications in the seismic design and collapse capacity of steel special moment frames. *Earthquake Eng. and*
631 *Structural Dynamics* 43:1935–1954. doi: 10.1002/eqe.2430
- 632 Elkady A, Lignos DG (2015) Effect of gravity framing on the overstrength and collapse capacity of steel frame buildings
633 with perimeter special moment frames. *Earthquake Eng. and Structural Dynamics* 44:1289–1307. doi:
634 10.1002/eqe.2519
- 635 Engelhardt M, Venti M, Fry G, et al (2000) Behavior and design of radius-cut reduced beam section connections. SAC Joint
636 Venture
- 637 Fardis MN (2018) Capacity Design: Early History. *Earthquake Eng. and Structural Dynamics*. doi: 10.1002/eqe.3110
- 638 Fujisawa K, Ichinohe Y, Sugimoto M, Sonoda M (2013) Statistical study on mechanical properties and chemical
639 compositions of SN Steels. In: *Summary of Technical Papers of Annual Meeting*. Architectural Institute of Japan,
640 pp 699–700
- 641 Hartloper A, Lignos D (2017) Updates to the ASCE 41-13 Provisions for the Nonlinear Modeling of Steel Wide Flange
642 Columns for performance-based earthquake engineering. In: *The 8th European Conference on Steel and Composite*
643 *Structures*. Copenhagen, Denmark
- 644 Hirofumi A, Masayuki M (1985) Statistical investigation on mechanical properties of structural steel based on coupon tests.
645 *J Struct Constr Eng AIJ* 94–105
- 646 Jones SL, Fry GT, Engelhardt MD (2002) Experimental evaluation of cyclically loaded reduced beam section moment
647 connections. *J Struct Eng* 128:441–451. doi: 10.1061/(ASCE)0733-9445(2002)128:4(441)

- This paper is published as :** El Jisr, H., Elkady, A., Lignos, D.G. (2019). “Composite steel beam database for seismic design and performance assessment of composite-steel moment-resisting frame systems, *Bulletin of Earthquake Engineering*, Vol. 17(6), pp. 3015-3039, doi: 10.1007/s10518-019-00564-w.
- 648 Kanno R (2016) Advances in steel materials for innovative and elegant steel structures in Japan—A Review. *Struct Eng Int*
649 26:242–253. doi: 10.2749/101686616X14555428759361
- 650 Kim KD, Engelhardt MD (2002) Monotonic and cyclic loading models for panel zones in steel moment frames. *J Constr*
651 *Steel Res* 58:605–635. doi: 10.1016/S0143-974X(01)00079-7
- 652 Kim S-Y, Lee C-H (2017) Seismic retrofit of welded steel moment connections with highly composite floor slabs. *J Constr*
653 *Steel Res* 139:62–68. doi: 10.1016/j.jcsr.2017.09.010
- 654 Kim Y-J, Oh S-H, Moon T-S (2004) Seismic behavior and retrofit of steel moment connections considering slab effects.
655 *Eng Struct* 26:1993–2005. doi: 10.1016/j.engstruct.2004.07.017
- 656 Kishiki S, Kadono D, Satsukawa K, Yamada S (2010) Consideration of composite effects on elasto-plastic behavior of
657 panel zone. *J Struct Constr Eng AIJ* 75:1527–1536
- 658 Krawinkler H (1978) Shear in beam-column joints in seismic design of steel frames. *Eng J* 15:82-91
- 659 Krawinkler H (2009) Loading histories for cyclic tests in support of performance assessment of structural components. In:
660 *The 3rd International Conference on Advances in Experimental Structural Engineering*. San Francisco
- 661 Lee C-H, Jeon S-W, Kim J-H, Uang C-M (2005) Effects of panel zone strength and beam web connection method on
662 seismic performance of reduced beam section steel moment connections. *J Struct Eng* 131:1854–1865. doi:
663 10.1061/(ASCE)0733-9445(2005)131:12(1854)
- 664 Lee CH, Jung JH, Kim SY, Kim JJ (2016) Investigation of composite slab effect on seismic performance of steel moment
665 connections. *J Constr Steel Res* 117:91–100. doi: 10.1016/j.jcsr.2015.10.004
- 666 Leon R (1990) Serviceability of composite floors. In: *Proceedings of the 1990 National Steel Construction Conference*.
667 AISC, p 18
- 668 Leon R, Alsamsam I (1993) Performance and serviceability of composite floors. In: *Structural Engineering in Natural*
669 *Hazards Mitigation*. ASCE, pp 1479–1484
- 670 Leon RT, Hajjar JF, Gustafson MA (1998) Seismic response of composite moment-resisting connections. I: Performance.
671 *J Struct Eng*.124:868–876. doi: 10.1061/(ASCE)0733-9445(1998)124:8(868)
- 672 Lignos DG, Hikino T, Matsuoka Y, Nakashima M (2013) Collapse assessment of steel moment frames based on E-Defense
673 full-scale shake table collapse tests. *J Struct Eng*.139:120–132. doi: 10.1061/(ASCE)ST.1943-541X.0000608
- 674 Lignos DG, Krawinkler H (2011) Deterioration modeling of steel components in support of collapse prediction of Steel
675 moment frames under earthquake loading. *J Struct Eng*. 137:1291–1302. doi: 10.1061/(ASCE)ST.1943-
676 541X.0000376
- 677 Lignos DG, Krawinkler H (2013) Development and utilization of structural component databases for performance-based
678 earthquake engineering. *J Struct Eng*.139:1382–1394. doi: 10.1061/(ASCE)ST.1943-541X.0000646
- 679 Lu L, Xu Y, Zheng H (2017) Investigation of composite action on seismic performance of weak-axis column bending
680 connections. *J Constr Steel Res* 129:286–300. doi: 10.1016/j.jcsr.2016.11.019
- 681 Mele E (2002) Moment resisting welded connections: an extensive review of design practice and experimental research in
682 USA, Japan and Europe. *J Earthquake Engineering* 06:111–145. doi: 10.1142/S1363246902000590
- 683 Nakashima M, Matsumiya T, Suita K, Liu D (2005) Test on full-scale three-storey steel moment frame and assessment of
684 ability of numerical simulation to trace cyclic inelastic behaviour. *Earthquake Eng. and Structural Dynamics* 35:3–
685 19. doi: 10.1002/eqe.528
- 686 Nakashima M, Matsumiya T, Suita K, Zhou F (2007) Full-Scale test of composite frame under large cyclic loading. *J Struct*
687 *Engineering* 133:297–304. doi: 10.1061/(ASCE)0733-9445(2007)133:2(297)
- 688 Nakashima M, Roeder C, Maruoka Y (2000) Steel moment frames for earthquakes in United States and Japan. *J Structural*
689 *Engineering* 126:861–868. doi: 10.1061/(ASCE)0733-9445(2000)126:8(861)
- 690 Nam T, Kasai K (2012) Study on shake table experimental results regarding composite action of a full-scale steel building
691 tested to collapse. In: *9th Int. Conference on Urban Earthquake Eng./4th Asia Conference on Earthquake*
692 *Engineering*. Tokyo Institute of Technology, Tokyo, pp 1111–1116
- 693 Panagiotakos TB, Fardis MN (2001) Deformations of reinforced concrete members at yielding and ultimate. *Struct J*
694 98:135–148
- 695 PEER/ATC (2010) Modeling and acceptance criteria for seismic design and analysis of tall buildings. *Applied Technology*
696 *Council (ATC)*, Redwood City, CA

This paper is published as : El Jisr, H., Elkady, A., Lignos, D.G. (2019). “Composite steel beam database for seismic design and performance assessment of composite-steel moment-resisting frame systems, *Bulletin of Earthquake Engineerin*, Vol. 17(6), pp. 3015-3039, doi: 10.1007/s10518-019-00564-w.

- 697 Ricles JM, Fisher JW, Lu L-W, Kaufmann EJ (2002) Development of improved welded moment connections for
698 earthquake-resistant design. *J Constr Steel Res* 58:565–604. doi: 10.1016/S0143-974X(01)00095-5
- 699 Roeder CW (2000) State of the art report on connection performance. Federal Emergency Management Agency,
700 Washington D.C.
- 701 Roeder CW (2002) General issues influencing connection performance. *J Structural Engineering* 128:420–428. doi:
702 10.1061/(ASCE)0733-9445(2002)128:4(420)
- 703 Shin, S., Engelhardt, M. D. (2013). Cyclic Performance of Deep Column Moment Frames with Weak Panel Zones. In:
704 *Advances in Structural Engineering and Mechanics (ASEM13)*, Jeju, Korea.
- 705 Suita K, Yamada S, Tada M, et al (2008) Collapse experiment on four-story steel moment frame: Part 2. In: *The 14th World*
706 *Conference on Earthquake Engineering*. Beijing
- 707 Sumner EA, Murray TM (2002) Behavior of extended end-plate moment connections subject to cyclic loading. *J Struct Eng*
708 128:501–508. doi: 10.1061/(ASCE)0733-9445(2002)128:4(501)
- 709 Tagawa Y, Kato B, Aoki H (1989) Behavior of composite beams in steel frame under hysteretic loading. *J Struct Eng*
710 115:2029–2045. doi: 10.1061/(ASCE)0733-9445(1989)115:8(2029)
- 711 Tremblay R, Tchebotarev N, Filiatrault A (1997) Seismic performance of RBS connections for steel moment resisting
712 frames: Influence of loading rate and floor slab. In: *Proceedings of Stessa*
- 713 Uang C-M, Yu Q-S, Noel S, Gross J (2000) Cyclic testing of steel moment connections rehabilitated with RBS or welded
714 haunch. *J Structure Engineering* 126:57–68. doi: 10.1061/(ASCE)0733-9445(2000)126:1(57)
- 715 Yamada S, Satsukawa K, Kishiki S, et al (2009) Elasto-plastic behavior of panel zone in beam to external column connection
716 with concrete slab. *J Struct Constr Eng AIJ* 74:1841–1849
- 717 Zhang X, Ricles J, Lu L-W, Fisher J (2004) Development of seismic guidelines for deep-column steel moment connections.
718 Lehigh University
719